Progress in Electrical Engineering and Applied Physics

Broadband Bandpass Filter Utilizing a Multi-Mode Resonator for Wireless Communication Applications

Fatima kiouach[1], Mohammed EL GHZAOUI[1]

[1]*Sidi Mohamed Ben Abdellah University, Faculty of Sciences, Fes, Morocco.*

Abstract

This paper presents a novel broadband bandpass filter that utilizes a multiple-mode resonator (MMR) for communication applications. The filter is designed using Rogers RT/duroid 5880 substrate, which has a relative permittivity of 2.2, a dielectric loss tangent of 0.0009, and a thickness of 0.8 mm. The design process was carried out using the High Frequency Structure Simulator (HFSS). The filter's overall dimensions are 14.8 x 2.9 mm². Simulated S-parameters indicate a bandwidth of 17.46 GHz (6.00 - 23.46 GHz) for the filter. It achieves a 3-dB fractional bandwidth (FBW) of 149.23%, an insertion loss of less than 0.2 dB, and a return loss greater than 48.85 dB, while maintaining a nearly constant group delay across the passband. These exceptional performance characteristics make it highly suitable for a variety of communication systems, including 5G (4–8 GHz), satellite communications, and radar systems operating in the X-band (8–12 GHz) and Ku-band (12–18 GHz).

Keyword: Broadband bandpass filter, MMR, HFSS, FBW.

1 Introduction

The rapid expansion of wireless communication systems has created an increasing demand for components capable of supporting broad frequency ranges with both high efficiency and reliability. Among these components, bandpass filters are essential, as they ensure signal integrity by allowing desired frequency bands to pass while suppressing unwanted interferences. To achieve wideband performance, Multi-Mode Resonators (MMRs) have emerged as a key technology and have garnered significant attention in recent years. By incorporating MMRs into filter designs, advanced characteristics such as low insertion loss and sharp roll-off can be achieved, addressing the stringent demands of high-performance wireless communication systems.

Recent research has focused on broadband bandpass filters for wireless communications. Ref. [1] proposes a broadband high-selectivity filter spanning 2.5-16.8 GHz with a wide bandwidth of about 14.3 GHz. The filter, offering a super-wideband response of 148.18% fractional bandwidth, low insertion loss of 0.4 dB, high return loss over 10 dB and out-of-band performance up to 25 GHz. These characteristics enable integration into upcoming wireless communication systems. Ref. [2] presents an ultra-wideband (UWB) bandpass filter with low insertion loss and compact size. The fabricated BPF operates at 6.85 GHz and demonstrates -0.6 dB insertion loss and 114% fractional bandwidth (FBW). A compact UWB bandpass filter, as described in Ref. [3], is designed using a Pythagorean tree fractal stub-loaded resonator. The filter features a compact size of 12.13 mm × 9.59 mm and achieves a stopband extension up to 17.5 GHz with a maximum attenuation of 15 dB. Ref. [4] introduces a novel UWB BPF using fractal tree stub loaded multimode resonators. The proposed filter demonstrates excellent performance, covering the full UWB range with low insertion loss and high return loss, while maintaining a compact size of 11.5 x 9.6 mm². Ref. [5] presents a compact UWB bandpass filter, offering low insertion loss and high selectivity. It covers the UWB range of 3.1–10.6 GHz with a -3dB fractional bandwidth of 110%, featuring multiple resonant frequencies and two transmission zeros. The paper referenced in [6] presents the design of a novel bandpass filter for 5G mm-Wave communications. This filter operates at a center frequency of 22.65 GHz with a 10.5 GHz bandwidth, achieving a reflection coefficient of -39.12 dB and an insertion loss of -0.59 dB. Ref. [7] presents a UWB bandpass filter with stopband characteristics, utilizing an MMR and defected ground structures to enhance bandwidth and roll-off rate. The filter achieves a group delay of less than 0.30 ns, and a roll-off rate of 16 dB/GHz. Ref.

[8] introduces a bandpass filter for ultra-wideband applications. The filter features low insertion loss (~0.8 dB), a bandwidth from 3.11 to 10.63 GHz, and a wide stopband. A BPF with a T-shaped stub structure is introduced in Ref. [9], achieving five transmission poles and eight transmission zeros (TZs). The filter operating at 2.05 GHz and shows rejection levels exceeding 45.5 dB in the lower stopband and 19.5 dB in the upper stopband. Ref. [10] presents an UWB-BPF, offers excellent passband performance (2.92–10.95 GHz, 107% FBW), effective spurious frequency suppression (>30 dB at $2f_0$), and compact size. In [11], a filter featuring a fractional bandwidth of 62.3% was developed utilizing a staircase-shaped resonator. This paper referenced [12] presents a balanced ultra-wideband bandpass filter with a compact, simple structure to achieve a 132% fractional bandwidth. A low-cost microstrip bandpass filter for 5G mid-band (3.7–4.2 GHz) applications presented in Ref. [13], on an FR4 substrate. The design achieves a fractional bandwidth of 12.8%, including a return loss >18 dB and insertion loss <2.5 dB.

This paper introduces an innovative broadband bandpass filter, specifically designed to meet the demanding requirements of modern communication systems. At the core of this design is the multiple-mode resonator (MMR), which plays a crucial role in enhancing the filter's performance for a wide range of communication applications. The filter is carefully constructed using Rogers RT/duroid 5880 substrate, with a relative permittivity of 2.2, a low dielectric loss tangent of 0.0009, and a thickness of 0.8 mm. The entire design process was carried out using the High Frequency Structure Simulator (HFSS), with an overall dimensions of 14.8 x 2.9 mm². Simulated S-parameters reveal that the filter boasts a remarkable bandwidth of 17.46 GHz, covering the frequency range from 6.00 GHz to 23.46 GHz, which ensures a wide operational range with exceptional selectivity. Moreover, the filter demonstrates impressive performance metrics, including a 3-dB fractional bandwidth (FBW) of 149.23%, an insertion loss that remains below 0.2 dB, and a return loss greater than 48.85 dB, ensuring minimal signal degradation and optimal energy transmission. Additionally, the group delay is remarkably stable across the entire passband, ensuring that the filter maintains signal integrity throughout its operational range.Given its outstanding characteristics, this filter is highly suited for a variety of advanced communication systems. Its wideband response and superior performance make it an excellent choice for next-generation applications, including 5G networks operating in the 4–8 GHz range, satellite communication systems, and radar applications within the X-band (8–12 GHz) and Ku-band (12–18 GHz), among others.

2 Design and Implementation of the Proposed Bandpass Filter

A bandpass filter was designed utilizing Rogers RT/duroid 5880 substrate, featuring a relative permittivity of 2.2 and a dielectric loss tangent of 0.0009. The High Frequency Structure Simulator (HFSS) was employed for the design process. The filter layout was positioned on the top surface of the substrate, with a comprehensive ground plane situated on the underside. Figure 1 illustrates the proposed bandpass filter geometry, comprising a ring multiple-mode resonator (MMR) coupled with interdigital lines and supported by a full ground plane. The overall dimensions of the filter were measured at 14.8 mm x 2.9 mm x 0.8 mm, as depicted in Figure 1.

Optimum dimensions were determined as follows: L1 = 0.4 mm, L2 = 0.1 mm, L3 = 2.0 mm, W1 = 2.0 mm, W2 = 3.4 mm, W3 = 10.6 mm, r = 1.1 mm, and r1 = 0.9 mm. The substrate dimensions were established at L_S = 14.8 mm and W_S = 2.9 mm, respectively.

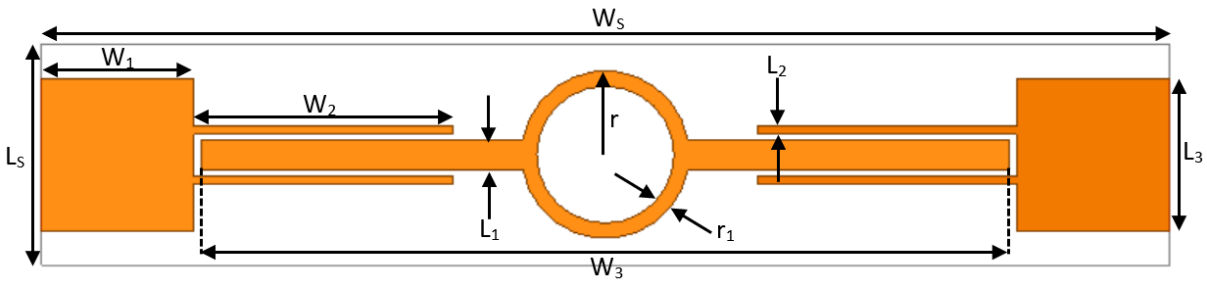

Figure 1. Top view of the proposed BPF design.

2.1 Theoretical Analysis of the Proposed Bandpass Filter

The proposed bandpass filter design (Figure 2) is symmetric, allowing for characterization using the even-odd mode analysis technique. This approach is especially beneficial for the theoretical analysis of multimode resonator (MMR). By utilizing the plane of symmetry, the even-odd mode analysis partitions the resonator into two subunits, greatly streamlining the analytical process.

The resonating element of the bandpass filter is initially illustrated in Figure 2 (a). During odd-mode or even-mode excitation, current diminishes along the plane of symmetry, resulting in equivalent circuit representations based on characteristic admittance and electrical length, as depicted in Figures 2 (b – c).

Key parameters in this configuration include:

- Characteristic admittances (Yi), where i = 1 and 2, which depend on the corresponding microstrip line width.
- Electrical lengths (θ_i), with i = 1 and 2, which are functions of their respective microstrip line lengths.

The electrical lengths θ_i (i = 1 and 2) are determined by:

$$\theta_i = \beta l_i \tag{1}$$

$$\beta = \frac{2\pi}{\lambda_g} \; and \; \lambda_g = \frac{c}{f\sqrt{\varepsilon_{re}}} \tag{2}$$

Here, l_i denotes the physical length of the respective microstrip line. For the ring resonator, the total length or circumference is given by 2πr. The term β denotes the phase constant, c represents the speed of light (3×10^8 m/s), λ_g is the guided wavelength, ε_{re} signifies the effective relative permittivity, and f stands for the frequency.

1. Equivalent Circuit for Even-Mode Excitation

The equivalent circuit depicted in Figure 2 (b) is applicable for even-mode excitation scenario. In this configuration, the plane of symmetry (T-T') is intentionally left open-circuited. Consequently, the input admittance for even-mode excitation can be expressed as follows:

$$Y_{in,even} = Y_1 \frac{Y_{in2} + jY_1 \tan\theta_1}{Y_1 + jY_{in2} \tan\theta_1} \tag{3}$$

Where:

$$Y_{in2} = jY_2 \tan\theta_2 \tag{4}$$

The condition governing resonance for even-mode excitation is characterized by a specific criterion:

$$Y_{in,even} = 0 \tag{5}$$

Which means for even-mode:

$$Y_1 \tan\theta_1 + Y_2 \tan\theta_2 = 0 \tag{6}$$

For simplicity, assuming Y_1=Y_2, the Equation (6) simplifies to the following condition:

$$\tan\theta_1 + \tan\theta_2 = 0 \tag{7}$$

From Equation (6), we determine that $\theta_1 + \theta_1 = n\pi$, where n=1,2,3 … For simplicity, we consider n = 1. Additionally, from Equations (1) and (2), we have:

$$\Theta_1 = \beta l_1, \Theta_2 = \beta l_2 \; and \; \beta = \frac{2\pi f\sqrt{\varepsilon_{re}}}{c} \tag{8}$$

Using, Equations (7), and (8), the expression of the resonance frequency for even-mode is derived as:

$$f_{even} = \frac{c}{2\,(l_1 + l_2)\sqrt{\varepsilon_{re}}} \tag{9}$$

2. Equivalent Circuit for Odd-Mode Excitation

The equivalent circuit for odd-mode analysis, depicted in Figure 2 (c). When subjected to odd-mode excitation, the plane of symmetry (T-T') becomes short-circuited. Consequently, the input admittance for odd-mode excitation can be expressed as follows:

$$Y_{in,odd} = -jY_1 \cot\theta_1 \tag{10}$$

The condition governing resonance for odd-mode excitation is characterized by a specific criterion:

$$Y_{in,odd} = 0 \tag{11}$$

Which means for odd-mode:

$$\cot\theta_1 = 0 \tag{12}$$

From Equation (7), we determine that $\theta_1 = \frac{n\pi}{2}$, where n=1,2,3 … For simplicity, we consider n = 1. Additionally, from Equations (1) and (2), we have:

$$\Theta_1 = \beta l_1 \; and \; \beta = \frac{2\pi f\sqrt{\varepsilon_{re}}}{c} \tag{13}$$

Using, Equations (12), and (13), the expression of the resonance frequency for odd-mode is derived as:

$$f_{odd} = \frac{c}{4l_1\sqrt{\varepsilon_{re}}} \tag{14}$$

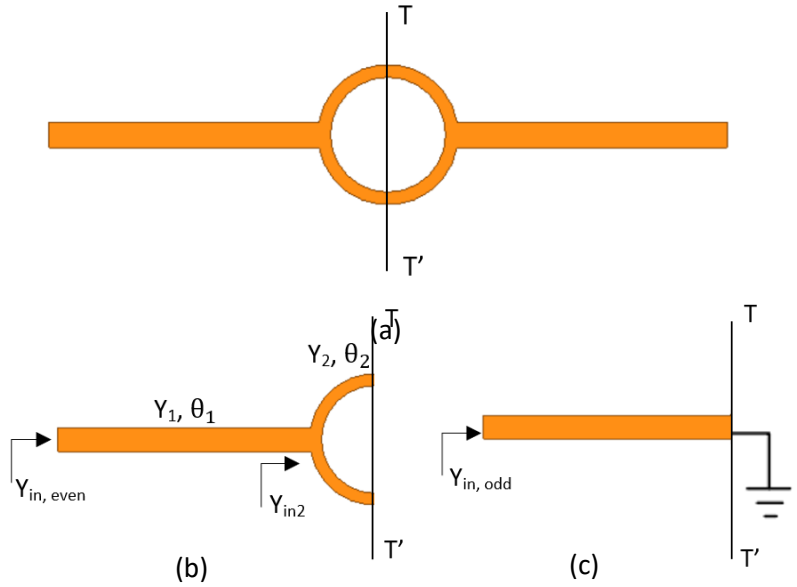

Figure 2. Equivalent circuit configuration: (a) Multimode resonator configuration (MMR) Unit of proposed design, (b) Even-mode and (c) Odd-mode.

2.2 Parametric Study

In this section, we examine the impact of parameter variations on the performance of the proposed bandpass filter. Each parameter is varied individually while keeping the others constant.

The first parameter analyzed is W_2. As illustrated in Figure 3(a), varying W_2 affects both the number of transmission zeros (TZs) and the S_{11} response. When W_2 is reduced from 3.4 mm to 3.2 mm, the maximum S_{11} value decreases from -48.85 dB to -44.25 dB. Further reduction to W_2 = 3 mm results in the number of TZs decreasing from 4 (at W_2=3.4 mm and W_2 = 3.2 mm) to 3, while the maximum S_{11} value decreases to -42.97 dB. When W_2 is reduced further to 2.8 mm, the number of TZs decreases to 2, and the S_{11} value slightly increases to -44.50 dB. Meanwhile, S_{21} remains stable across the variation of W_2, as shown in Figure 3(b). Based on these observations, the optimal value for W_2 is determined to be 3.4 mm.

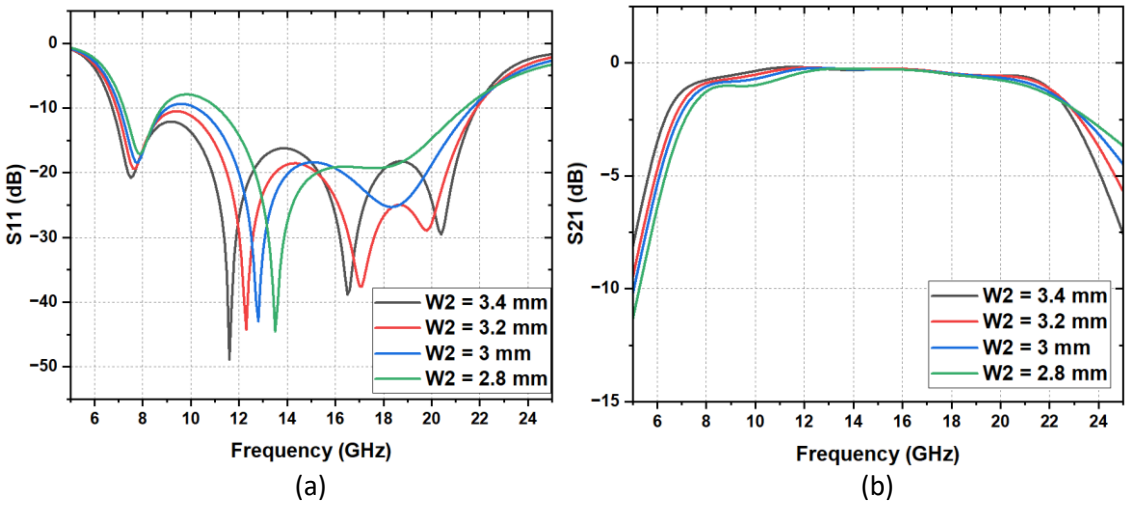

Figure 3. Impact of W2 variation on the (a) S_{11}, and (b) S_{21} of the proposed bandpass filter.

Varying W_3 influences both the S_{11} response and the bandwidth, as illustrated in Figure 4(a). When W_3 is reduced from 10.6 mm to 9.7 mm, the maximum S_{11} value increases from -48.85 dB to -41.7 dB,

indicating reduced impedance matching. Additionally, a slight increase in bandwidth is observed as W_3 decreases, while the number of transmission zeros (TZs) remains unaffected by changes in W_3. Meanwhile, as shown in Figure 4(b), S_{21} remains stable across the variations in W_3. Based on these observations, the optimal value for W_3 is determined to be 10.6 mm.

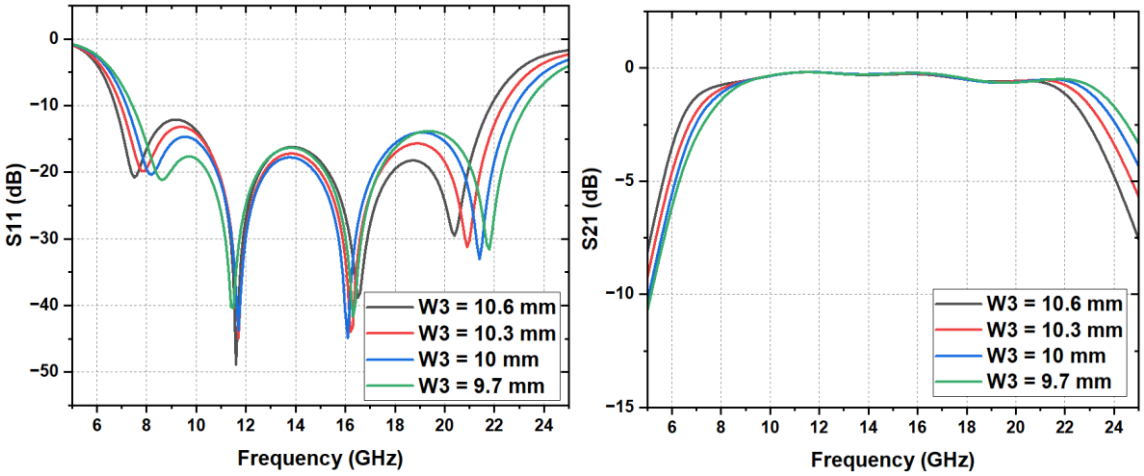

(a) (b)

Figure 4. Impact of W3 variation on the (a) S11, and (b) S21 of the proposed bandpass filter.

Figure 5(a) illustrates the impact of varying L_1 on the S_{11} response, transmission zeros (TZs), and bandwidth. When L_1 is reduced from 0.4 mm to 0.1 mm results in an increase in the maximum S11 value from -48.85 dB to -28.35 dB, indicating a degradation in impedance matching. Changes in L_1 also reduce the number of transmission zeros, while the bandwidth decreases from 17.46 GHz to 11.8 GHz. Figure 5(b) shows that S_{21} exhibits minimal change across variations in L_1. Based on these findings, the optimal value for L_1 is identified as 0.4 mm.

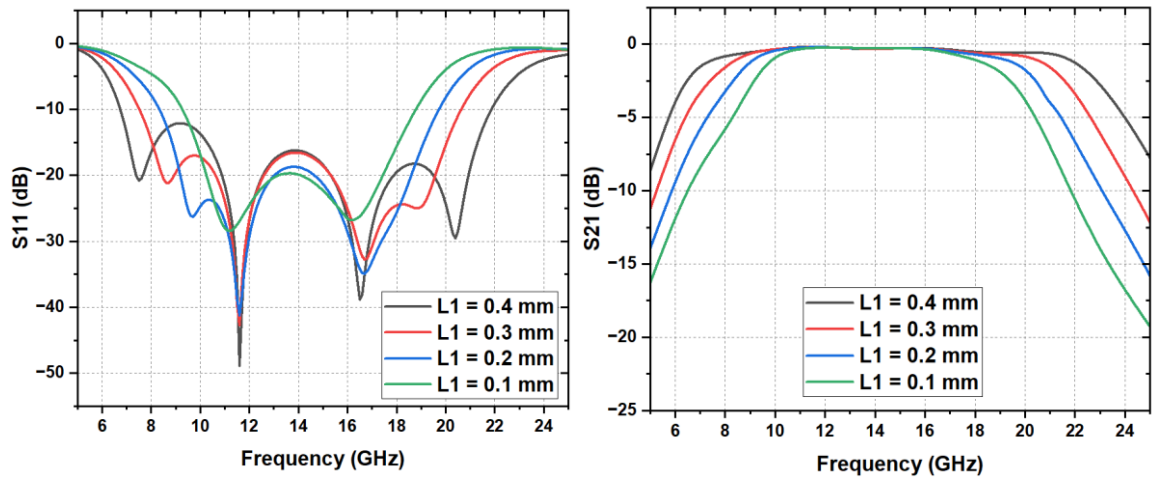

(a) (b)

Figure 5. Impact of L1 variation on the (a) S11, and (b) S21 of the proposed bandpass filter.

Figure 6(a) demonstrates the impact of varying L_2 on the S_{11} response, transmission zeros (TZs), and bandwidth. As L_2 increases from 0.1 mm to 0.25 mm, the maximum S_{11} value rises from -48.85 dB to -30.79 dB. Further increases to 0.4 mm and 0.55 mm result in a slight improvement, with the maximum S_{11} reaching -37.04 dB for both values. Additionally, increasing L_2 reduces the number of transmission zeros from 4 to 2 and decreases the bandwidth from 17.46 GHz to 15.60 GHz. Figure 6(b) reveals that S_{21} remains largely unaffected by variations in L_2. Based on these findings, the optimal value for L_2 is determined to be 0.1 mm.

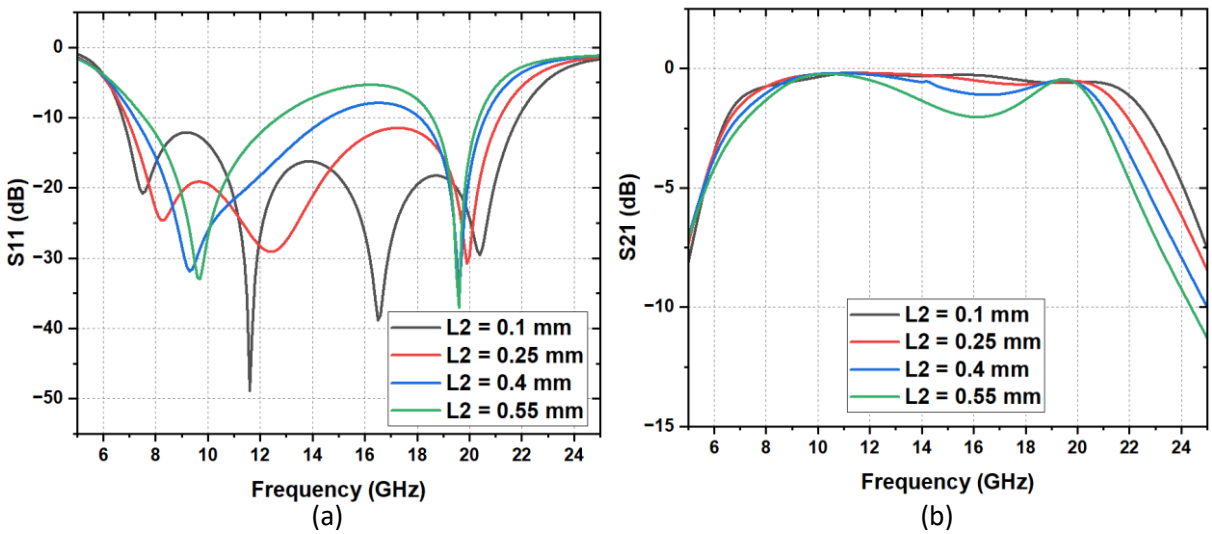

Figure 6. Impact of L2 variation on the (a) S11, and (b) S21 of the proposed bandpass filter.

The final parameter considered in this parametric study is r, the radius of the ring resonator. Figure 7(a) illustrates the effect of varying r on the filter's performance. As r increases from 1.1 mm to 1.2 mm, the maximum S_{11} value rises from -48.85 dB to -44.68 dB. A further increase to 1.3 mm slightly improves the performance, with S_{11} reaching -49.69 dB, before declining again to -45.21 dB when r is increased to 1.4 mm. Additionally, increasing r reduces the number of transmission zeros (TZs) from 4 to 2 and narrows the bandwidth from 17.46 GHz to 16.60 GHz. Figure 7(b) shows that S_{21} remains largely unaffected by variations in r. Based on these results, the optimal value of r is determined to be 1.1 mm.

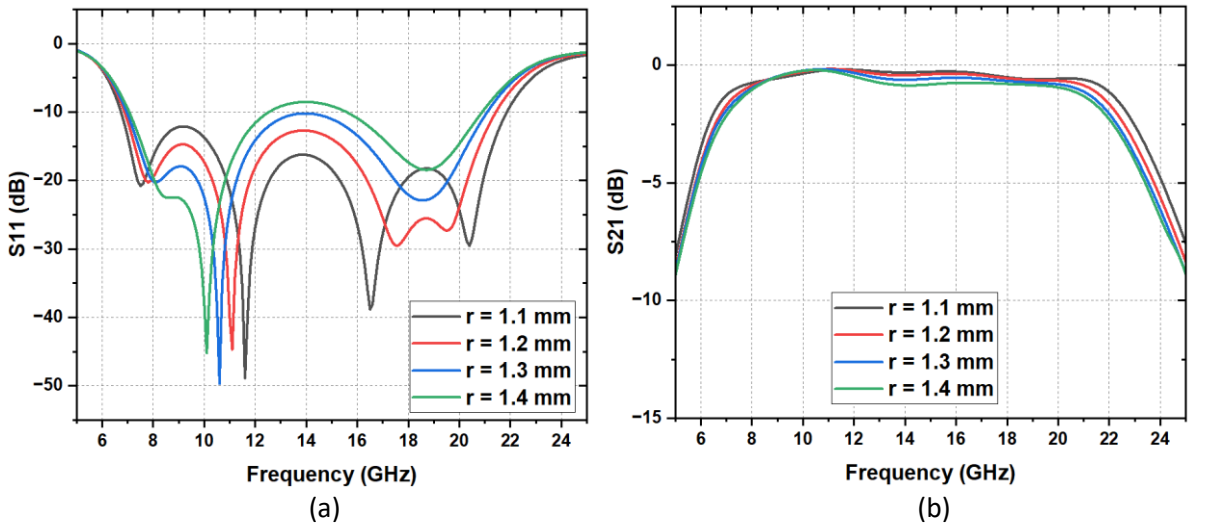

Figure 7. Impact of r variation on the (a) S11, and (b) S21 of the proposed bandpass filter.

3 Results and Discussions

This section presents an analysis of the results for the proposed bandpass filter, simulated using HFSS. The evaluation includes parameters such as S_{11}, S_{21}, group delay, and phase responses.

Figure 8 depicts the simulated S-parameters of the designed bandpass filter, which demonstrates a bandwidth of 17.46 GHz (ranging from 6.00 GHz to 23.46 GHz). The filter achieves a 3-dB fractional bandwidth (FBW) of 149.23%, an insertion loss below 0.2 dB, and a return loss greater than 48.85 dB.

In filter design, it is crucial to ensure consistent group delay (τ_d) and phase velocity (ϕ) throughout the passband to minimize frequency distortion. These parameters can be expressed as follows [14]:

$$\tau_d = \frac{d\varphi_{21}(\omega)}{-d\omega} \tag{15}$$

$$\varphi_{21}(\omega) = \arg S_{21}(\omega) \tag{16}$$

In the equations, ϕ_{21} and τ_d represent phase and group delay, respectively, in relation to the magnitude S_{21}. As shown in Figure 9(a), the group delay remains nearly constant across the entire passband, ensuring uniform current flow with consistent velocity and phase, thereby minimizing frequency dispersion. Furthermore, Figure 9(b) illustrates the phase response of the proposed bandpass filter.

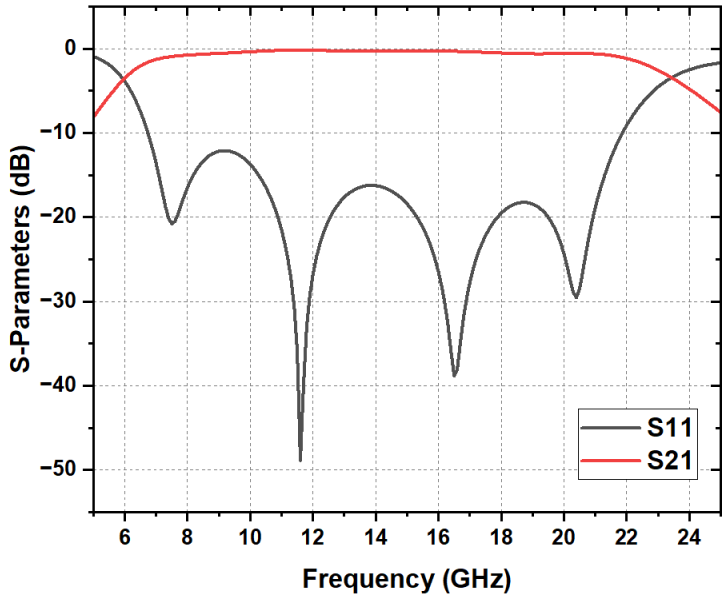

Figure 8. S-Parameters results of the proposed bandpass filter.

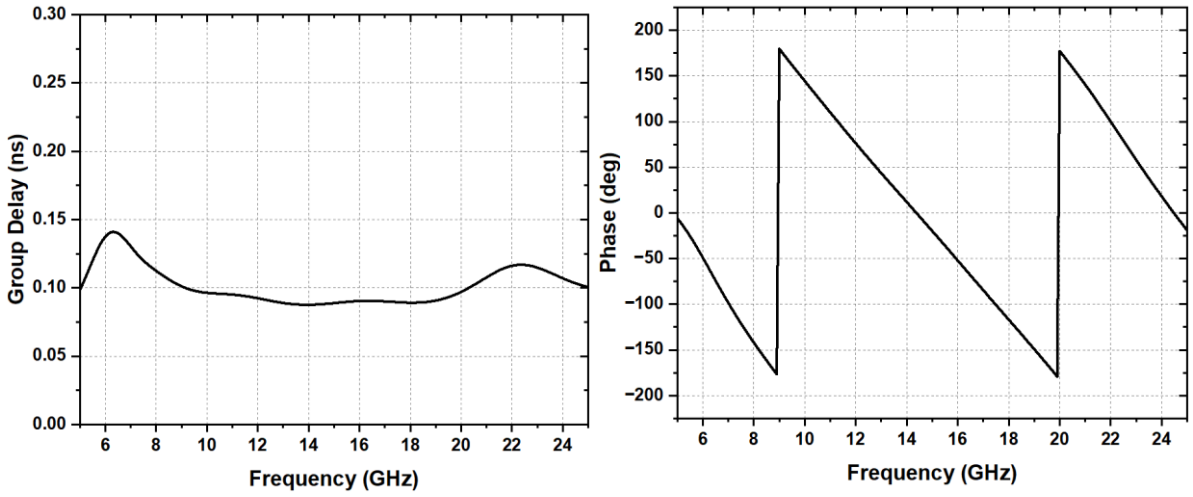

(a) (b)

Figure 9. (a) Group delay and (b) Phase responses of the proposed BPF.

4 Comparison of the Proposed BPF with other Works

Table 1 present a Comparison between the proposed BPF and other works. The proposed bandpass filter presented in this work outperforms previous designs in several aspects. It offers the widest bandwidth 17.46 GHz (6.00–23.46 GHz), with the highest 3-dB fractional bandwidth (FBW) of 149.23%, surpassing all other references. For instance, while Reference 1 has the closest FBW of 148.18%, it operates over a narrower band (2.50–16.80 GHz). The filter also achieves an exceptionally low insertion loss (IL) of less than 0.20 dB, outperforming others such as Reference 12 (<2.50 dB) and Reference 13 (<2.40 dB). Even designs with lower IL values, like Reference 5 (<0.35 dB), fall short of the overall performance of this work.

The return loss (RL) exceeds 48.85 dB, significantly higher than any other reference, such as Reference 5, which achieves >21.70 dB, or most other designs offering RL values >10.00 dB. This highlights the superior impedance matching and reflection suppression of the proposed filter. Furthermore, the design maintains a compact size of 14.80 × 2.90 mm, making it the smallest among all references. Reference 10, which has a size of 10.09 × 12.04 mm, offers a narrower passband (2.92–10.95 GHz), lower FBW (107%), and higher IL (<0.49 dB).

This work demonstrates advancements in bandwidth, fractional bandwidth, and return loss. Its outstanding performance makes it highly suitable for various communication systems, including 5G (4–8 GHz), satellite communications, and radar systems in the X-band (8–12 GHz) and Ku-band (12–18 GHz).

Table 1. Comparison of the proposed BPF with other works.

Ref. Year of Publication	Passband (GHz)	3-dB FBW (%)	IL (dB)	RL (dB)	Filter size (mm×mm)
1 (2023)	2.50–16.80	148.18	<0.40	>10.00	22.50 × 12.00
2 (2022)	2.95–10.75	113.90	<0.60	>14.00	11.50 × 9.80
3 (2021)	3.60–10.40	103.90	<1.50	>10.00	12.13 × 9.59
4 (2021)	3.70–9.60	106.20	<1.00	>10.00	11.50 × 9.60
5 (2022)	3.10–10.60	110.00	<0.35	>21.70	28.40 × 7.80
7 (2021)	3.10–10.60	109.00	<0.40	>20.00	22.00 × 20.00
8 (2020)	3.21–10.77	109.40	<0.80	>15.00	23.40 × 10.00
10 (2021)	2.92–10.95	107.00	<0.49	>12.00	10.09 × 12.04
12 (2021)	2.70–8.23	132.00	<2 .50	>10.00	32.00 × 15.00
13 (2021)	3.70–4.20	12.66	<2 .40	>18.00	25.00 × 50.00
This Work (2025)	6.00–23.46	149.23	<0.20	>48.85	14.80 × 2.90

5 Conclusion

A novel broadband bandpass filter has been developed using a multiple-mode resonator (MMR) in this work. The design process was carried out using the High Frequency Structure Simulator (HFSS) software with overall dimensions of 14.8 x 2.9 x 0.8 mm³. Rogers RT/duroid 5880 substrate was employed, which has a relative permittivity of 2.2 and a dielectric loss tangent of 0.0009. Simulation results demonstrate a wide bandwidth of 17.46 GHz (6.00 - 23.46 GHz) with a 3-dB fractional bandwidth of 149.23%, an insertion loss below 0.2 dB, and a return loss exceeding 48.85 dB. The filter maintains nearly constant group delay across the passband. These characteristics make it suitable for various communication systems, including 5G networks, satellite communications, and radar systems.

References

[1] Basit, A., Daraz, A., & Zhang, G. (2023). Implementation of a Wideband Microwave Filter Design with Dual Electromagnetic Interference (EMI) Mitigation for Modern Wireless Communication Systems with Low Insertion Loss and High Selectivity. Micromachines, 14(11), 1986. DOI : 10.3390/mi14111986.

[2] Xie, J., Tang, D., Shu, Y., & Luo, X. (2022). Compact UWB BPF with broad stopband based on loaded-stub and C-shape SIDGS resonators. IEEE Microwave and Wireless Components Letters, 32(5), 383-386. DOI : 10.1109/LMWC.2021.3136561.

[3] Kumari, P., Sarkar, P., & Ghatak, R. (2021). A Pythagorean tree fractal shape stub-loaded resonator as a UWB bandpass filter with wide stopband. International Journal of Microwave and Wireless Technologies, 13(5), 442-446. DOI : https://doi.org/10.1017/S1759078720001750.

[4] Kumari, P., Sarkar, P., & Ghatak, R. (2021). Design of a compact UWB BPF with a fractal tree stub loaded multimode resonator. IET Microwaves, Antennas & Propagation, 15(1), 55-61. DOI : 10.1049/mia2.12025.

[5] Ramanujam, P., Arumugam, C., Venkatesan PG, R., & Ponnusamy, M. (2022). Design of compact UWB filter using parallel-coupled line and circular open-circuited stubs. IETE Journal of Research, 68(6), 4665-4672. DOI : 10.1080/03772063.2020.1803772.DOI: 10.1080/03772063.2020.1803772.

[6] Kiouach, F., Aghoutane, B., & El Ghzaoui, M. (2023). Novel Microstrip Bandpass Filter for 5G mm-Wave wireless communications. e-Prime-Advances in Electrical Engineering, Electronics and Energy, 6, 100357. DOI : 10.1016/j.prime.2023.100357.

[7] Saxena, G., Jain, P., & Awasthi, Y. K. (2021). Design and analysis of a planar UWB bandpass filter with stopband characteristics using MMR technique. International Journal of Microwave and Wireless Technologies, 13(10), 999-1006. DOI : 10.1017/S1759078720001762.

[8] Shome, P. P., & Khan, T. (2020). A quintuple mode resonator based bandpass filter for ultra-wideband applications. Microsystem Technologies, 26(7), 2295-2304. DOI : 10.1007/s00542-019-04697-5.

[9] Xu, K. D., Lu, S., Ren, Y., Zhang, A., & Chen, Q. (2020). Coupled-line band-pass filter with T-shaped structure for high frequency selectivity and stopband rejection. International Journal of RF and Microwave Computer-Aided Engineering, 30(8), e22259. DOI: 10.1002/mmce.22259.

[10] Jamsai, M., Angkawisittpan, N., & Nuan-On, A. (2021). Design of a compact ultra-wideband bandpass filter using inductively compensated parallel-coupled lines. Electronics, 10(21), 2575. DOI : 10.3390/electronics10212575.

[11] Widaa, A., You, C. J., Awad, M., & Cai, J. (2021, January). Compact Wideband Bandpass Filter Using Miniaturized Staircase Interdigital Resonators. In 2020 50th European Microwave Conference (EuMC) (pp. 97-99). IEEE. DOI : 10.23919/EuMC48046.2021.9337995.

[12] Sun, J., & Li, G. R. (2021). A balanced ultra-wideband bandpass filter based on H-type sandwich slotline. International Journal of RF and Microwave Computer-Aided Engineering, 31(5), e22611. DOI: 10.1002/mmce.22611.

[13] Alnahwi, F. M., Al-Yasir, Y. I., Abdulhameed, A. A., Abdullah, A. S., & Abd-Alhameed, R. A. (2021). A low-cost microwave filter with improved passband and stopband characteristics using stub loaded multiple mode resonator for 5G mid-band applications. Electronics, 10(4), 450. DOI : 10.3390/electronics10040450.

[14] Zhang, G., Basit, A., Khan, M. I., Daraz, A., Saqib, N., & Zubir, F. (2023). Multi frequency controllable in-band suppressions in a broad bandwidth microstrip filter design for 5G Wi-Fi and satellite communication systems utilizing a quad-mode stub-loaded resonator. Micromachines, 14(4), 866. DOI : 10.3390/mi14040866.